Russian Chemical Reviews **62** (5) 409–418 (1993)
© 1993 Russian Academy of Sciences and Turpion Ltd

UDC 539.211 + 542.973 + 541.128

Studies of heterogeneous catalytic systems and of their models by scanning tunnelling microscopy

Sh K Shaikhutdinov, D I Kochubei

Contents

I. Introduction	409
II. Principles of the scanning tunnelling microscopy method	410
III. Studies of surfaces by scanning tunnelling microscopy	410

Abstract. Studies of carbon materials, oxides, metals, clusters, and model catalysts, of potential interest in the field of heterogeneous catalysis, are reviewed. The principles of the method and its possible applications are discussed. 127 references.

I. Introduction

Progress in heterogeneous catalysis is largely dependent on improvements in our understanding, at the molecular level, of surface structures and of surface processes. Various methods of studying surfaces are used for this purpose. Workers in this field have tried for many years to see atoms by observations in an optical microscope. This visualisation of the surface structure at the atomic level was made possible by the development, in 1981, of scanning tunnelling microscopy (STM).[1]

The principle of the STM effect is based on recording the tunnelling current between the sample and a needle scanning the sample surface (Figure 1). We know that in the case of a one-dimensional potential barrier[2] the tunnelling current is exponentially dependent on the width and height of the barrier (the distance between the tip of the needle and the surface, i.e. the tunnelling length, and the work function of the sample and needle materials respectively). This exponential dependence accounts for the high resolving power of the STM method (~ 1 Å in the plane of the surface and 0.1 Å at right angles to it). Furthermore, studies by STM offer the additional advantage that the measurements are non-destructive, are aimed at the surface layer itself, and can be made in liquids and in gases as well as in a vacuum. The main weaknesses of the method, which limit the range of applications of STM, include the stringent elimination of all mechanical vibrations, the small size (up to 10 μm^2) of the scanning region, and (perhaps most importantly) the fact that the measurements are confined to electrically conducting samples. The latter limitation provided a stimulus for the development of a whole family of new microscopes based on the STM concept: these include the atomic force microscope, which can be used with non-conducting as well as with conducting materials, the magnetic force microscope, the thermal microscope, and others.[3]

Recent studies of scanning tunnelling microscopy and of similar methods of surface analysis have shown that the analytical possibilities of these techniques are increasingly wide-ranging.[4, 5]

In spite of many suggestions of potential applications of STM in studies of catalytic systems, the first reports of studies of actual catalysts have only recently appeared. Evidently, difficulties have been encountered firstly because heterogeneous catalysts usually consist of a multiphased system on a highly dispersed (and often non-conducting) carrier, and secondly because at present surface structures are studied by STM without an element analysis. Therefore research must be confined to model systems consisting of metal single crystals, small particles on a conducting substrate, metal oxides, and carbonaceous materials. The present review is aimed at materials of these types.

STM began to be used here later than in some other countries, and this partly accounts for our lag in this field. We hope that this review will stimulate the interest of Russian physical chemists and encourage them to study by STM the atomic structure of reactions on surfaces more widely.

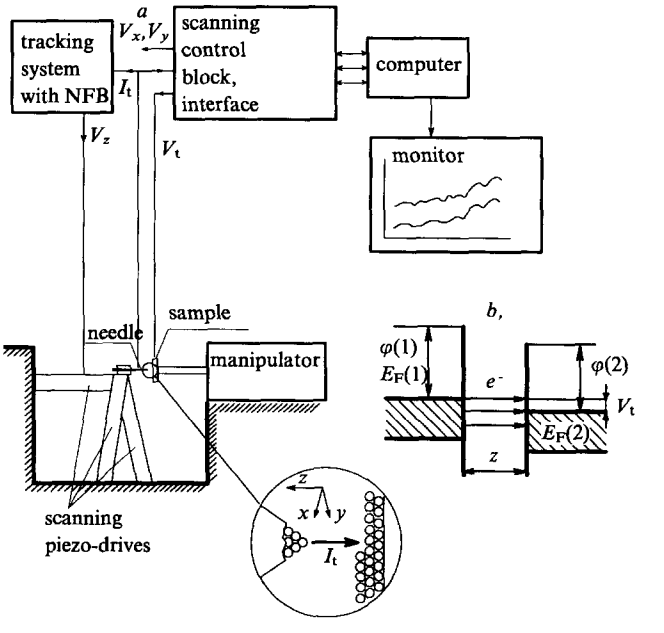


Figure 1. Block diagram of the STM (*a*) and schematic representation of the tunnelling process between the metallic needle and the sample (*b*). E_F is the Fermi energy, φ is the work function of the sample, V_t is the tunnelling voltage, I_t is the tunnelling current, z is the tunnelling distance, $V_{x,y}$ is the voltage applied to the scanning piezo-drives, V_z is the voltage applied to the z piezo-drives of the feedback system.

Sh K Shaikhutdinov, D I Kochubei G K Boreskov Institute of Catalysis, Siberian Section of the Russian Academy of Sciences, prosp. ak. Lavrent'eva 5, 630090, Novosibirsk. Fax (7-383-2) 35 57 56

Received 16th March 1993
Uspekhi Khimii **62** (5) 443–454 (1993); translated by J I Carasso

II. Principles of the scanning tunnelling microscopy method

Various types of STM have already been developed, including designs in which tunnelling microscopy is combined with other analytical methods of surface analysis.[6-8] A block diagram of an STM and of its component parts is shown † in Figure 1. Elements common to all types of STM include a vibration isolation system, which limits the amplitude of external perturbations of the tunnelling length to 0.05 Å; a system which allows the needle to be brought gradually closer to the surface until a tunnel current is obtained; an electronic system with negative feedback (NFB), which maintains the required tunnel current; a scanning needle with a tip having the smallest possible radius of curvature (ideally, terminating in a single atom), which mainly determines the spatial resolution of the apparatus; a frame scanning apparatus, based on piezoelectric ceramics (piezo-drives); a computer system for controlling the scan and for collecting and processing the required data.

In the topographic regime the negative feedback loop keeps the tunnel current constant throughout the scan. Under these conditions the vertical displacement Δz of the piezo-drive relative to the scanning plane reflects the geometry of the surface, and the STM picture is a $\Delta z(x, y)$ representation. In the fast scanning (constant height) regime the negative feedback loop does not follow the outline of the surface, and under these conditions the changes in the tunnel current ΔI are recorded, and the structure of the surface is obtained as a $\Delta I(x, y)$ representation. The latter regime can be used with relatively smooth surfaces, as in layer structures or single crystals, on which collisions between the needle and the surface are less likely.

An absolute calibration of the three-dimensional STM representation is usually obtained with samples of highly oriented pyrolytic graphite or samples containing monoatomic steps.

Obviously, the one-dimensional tunnelling model is a simplified first approximation which offers a qualitative interpretation of the STM picture. Attempts to develop a theory of three-dimensional tunnelling have met serious computational difficulties.

The tunnel current under conditions of weak binding between the electronic states on the surface of the needle and the sample is given by the expression[9]

$$I \approx \int_{-\infty}^{\infty} \rho_s(E+eV)\rho_t(E)|M(E)|^2[f(E)-f(E+eV)]\mathrm{d}E, \quad (1)$$

where E is the energy of a given electronic state, M is a matrix element of the electronic transition, $f(E)$ is the Fermi function, $\rho(E)$ is the state density function in the sample (s) and in the needle (t), and V is the tunnelling voltage.

At low voltages, and on the assumption that the point of the needle can be described by a hemisphere with its centre at the point $\mathbf{r}$ and that the wave function which describes the electronic structure of the surface has the form of an s-type atomic function, formula (1) can be simplified to[10,11]

$$I \sim V\rho_s(\mathbf{r}, E_F)\rho_t(E_F), \quad (2)$$

where $\rho_s(\mathbf{r}, E_F)$ and $\rho_t(E_F)$ are the densities of states at the Fermi level in the sample and in the needle respectively.

It is clear from Eqn (2) that in the topographic regime (I = const) the z-displacement of the STM needle, for which $\rho_t(x, y)$ is constant during the scan, takes place over a contour of constant local density of electronic states on the sample surface.

The results obtained by STM reflect not so much the geometric topography of the surface as its electronic structure, which is itself determined by the arrangement of the atoms. For example, the true position of the carbon atoms on the STM picture of the graphite surface is unquestionable. However, the image of a single atom adsorbed on an ideally smooth surface scanned by an atomically sharp needle can have different heights, depending on the tunnelling voltage, and it can even appear as a hollow.[12,13] This is due to the dependence of the electronic state density on the applied tunnelling voltage [see Eqn (1)]. This phenomenon complicates the interpretation of the observed STM picture, but it also allows the surface states to be probed. For small needle potentials, expressions of the following general form have been obtained for the differential conductivity:[14,15,18]

$$\frac{\mathrm{d}I}{\mathrm{d}V} \sim \rho_s(\mathbf{r}, V)T(V),$$

where $T(V)$ is the transparency of the barrier for a tunnelling voltage V.

By establishing the dependence of the tunnel current on the voltage we can measure the density of electronic states above and below the Fermi level, and in particular we can obtain direct information on the position of the energy gap in semiconductors. Experimentally this is done by suppressing the negative feedback during the time needed to measure the current–voltage characteristic. If this procedure is applied at all the scanning points on the surface the method is called scanning tunnelling spectroscopy (STS). It has yielded spectroscopic representations $[I(x, y, V)]$ of Si(111)–(7×7)[16,17] and GaAs(110)–(1×2) structures,[18] from which the atoms on the surface could be identified.

Thus more detailed information on the structure of the surface can be obtained by recording the STM image for different values of the tunnel voltage.

The parameters which mainly determine the tunnelling by electrons are the height and shape of the tunnel barrier. From the simplified formula for the tunnelling current

$$I \propto V\exp(-a z\sqrt{\varphi}),$$

where a is a constant, it follows that the average barrier height φ can be determined by measuring the changes in barrier current (ΔI) produced by changes in the tunnelling distance z,

$$\varphi \approx \left(\frac{\Delta \ln I}{\Delta z}\right)^2.$$

The work function of the material of the sample is obtained in this way.[2] These measurements are usually made by the phase detection method: this gives the STM representation as a $\varphi(x, y)$ dependence, which often offers a contrast better than that of a $\Delta z(x, y)$ topogram of the surface. It should be noted that the measured absolute values of the work function are often much lower than the known values, even when the experiment is carried out in a high vacuum. Usually this is attributed to adsorbates on the surface of the sample or of the needle.[19] Another possible explanation is that at short distances between the needle and the sample the height of the barrier decreases until a point contact is produced.[20-22]

Thus in order to analyse the processes taking place in STM and the experimental results obtained by this method we require additional information, including new theoretical models of the electronic structure of the surface.

III. Studies of surfaces by scanning tunnelling microscopy

1. Carbon materials

Highly oriented pyrolytic graphite (HOPG) is one of the materials most extensively studied by scanning tunnelling microscopy. It offers a number of advantages for the development of the STM technique, including a flat hexagonal layer structure extending over thousands of angstroms, and it is chemically inert. Nevertheless the STM pictures show some unusual features even for this relatively simple material.

Thus, samples of HOPG have shown an anomalously high atomic corrugation (the Δz_{max} value for an atomically flat surface

†The present writers have constructed an STM on the basis of an SO-03 Auger spectrometer.

with periodic packing), making neighbouring atoms non-equivalent in the STM picture and producing a trigonal rather than hexagonal symmetry in the resulting map.[23, 24]

One possible explanation of the anomalous corrugation, reaching ~1 Å, is that the tunnelling current is proportional to the local density of electronic states. According to theoretical calculations[11, 14, 25] the contours of constant density of states at the Fermi level show corrugations with an amplitude of ~0.8 Å, whereas in the total charge density contours the corrugations are only 0.2 Å high.

However, giant corrugations up to 8 Å in amplitude are often observed: these cannot be explained in terms of changes in the local charge density. One explanation proposed for this phenomenon assumes that at small tunnelling distances the interaction between the point and the sample produces elastic shifts of the surface atoms of graphite, and thus enhances the observed amplitude of the corrugations.[26] An alternative explanation relies on the shift of impurities and adsorbates (rather than of the graphite atoms themselves) on the surface of the sample or of the needle. Thus, it has been shown by electron microscopy[27] that when graphite is scanned in air microscopic carbon whiskers are formed on the tip of the needle: their deformation under the action of interatomic forces centred on the sample is assumed to result in giant corrugations.

The apparently trigonal symmetry of the basal plane of HOPG is usually attributed to the asymmetry of the local charge density distribution between neighbouring atoms. The local electron density on the surface is lower on the carbon atoms located above the atoms of the second layer, and therefore their image is suppressed in the STM picture.[28]

Another special feature of HOPG is the presence of surface superstructures, detected as a regular variation of the amplitude of the atomic corrugation of the graphite.[29–32] The lattice periodicity of the superstructures can reach hundreds of angstroms. Evidently, these superstructures can be classified into two groups.[33] The first includes superstructures whose period and amplitude depend on the angular mismatch between neighbouring graphite layers. In this case the STM picture reflects a real property of the surface: the difference in azimuthal orientation between the first two layers of graphite atoms. In the second group we find superstructures with constant period and amplitude, which show a sharp transition to the normal graphite structure. In this case the STM picture does not reflect the real structure of the surface: it is due to the presence on the tip of the needle of a crystalline graphite layer plane-parallel to the surface. The second class of superstructures is the more common, suggesting ready contamination of the point.

Effects arising from the formation of structures differing from the normal graphite structure can complicate the study of molecules adsorbed on HOPG, especially when the adsorbate is accommodated with a periodic packing.

The symmetry type of the STM picture of HOPG is determined by the electronic structure of the neighbouring carbon atoms, which is strongly influenced (as was pointed out above) by their interaction with the atoms of the underlying layer. This effect has been allowed for[34–39] in studies of graphite intercalation compounds (GIC) whose Fermi surface was controlled[40] by introducing electron donors or acceptors.

Thus, the STM pictures[34] of a GIC of the donor type (MC_8, M = K, Rb, Cs) show a 2×2 structure over a wide range of tunnel voltage and current (Figures 2*a* and 2*b*), determined by the distribution in space of a layer of donors under a layer of graphite.[37, 38] In the $CuCl_2$–HOPG system, which contains a GIC of the acceptor type,[35] the STM picture depended on the sign of the tunnelling voltage. When the electrons are tunnelling from the needle into the sample (at the electron localisation sites shown in Figure 2*d*) the STM picture has a clearly developed hexagonal symmetry. This indicates equivalence of the carbon atoms in the elementary cell of the basal plane, corresponding to a large decrease in the interaction between planes. When the polarity is inverted the STM picture is determined by the layer of acceptors and by their distribution under the upper graphite layer. However, a similar dependence of the STM image on the sign of the applied voltage is not found in compounds of graphite with electron donors. This means that in GIC of the donor type both occupied and unoccupied states are present near the Fermi level, and can contribute to the tunnelling. In the case of intercalation by a donor the charge transfer is relatively large, and if the packing of the donor layer matches that of the graphite the modulation of the electron density in the surface layer by the intercalated metal is more marked than in compounds of the acceptor type, in which the charge transfer is small and the packing is unmatched.[35]

A study of the $KHgC_4$ and $KHgC_8$ systems detected[39] a matched 2×2 superstructure in addition to the hexagonal graphite structure. This work led to the conclusion[34, 39] that the 2×2 structure is the result of a periodic arrangement of the potassium ions beneath a graphite layer. Furthermore a new orthorhombic superlattice was detected for the $KHgC_8$ complex, with parameters $a = b = 8.9$ Å and $\angle\gamma = 89°$, whose orientation is independent of the orientation of the graphite lattice. This structure is believed to be related to the waves of charge density observed in layer systems based on metal chalcogenides.

It can be seen that tunnelling microscopy offers valuable new information in studies of intercalation compounds.

Important new topics in the study of carbon materials include defect structures on the surface, the processes induced by bombarding the surface with various particles, and the amorphisation of graphite.[41–44] In particular, treating pyrolytic graphite with a methane plasma in a high-frequency discharge produces a strong modification of the surface:[44] the bombardment by the plasma ions yields amorphous formations ~50 Å in diameter which increase in number (but not in size) as the exposure time is increased. Obviously, regions of amorphous carbon are formed on defects induced by the plasma ions. In samples which had not been bombarded reproducible patterns could not be obtained because the operation of the STM was destabilised by the formation of an electrically insulating layer on the surface.

Recently reported[45–49] studies of other carbon materials have greater practical interest than the studies of HOPG. Thus, graphite structures obtained by the pyrolysis of various hydrocarbons have been examined,[45, 46] as well as carbon fibres.[47, 49] As could have been expected, pyrolytic graphites have a planar structure, but unlike the HOPG they contain large structurally

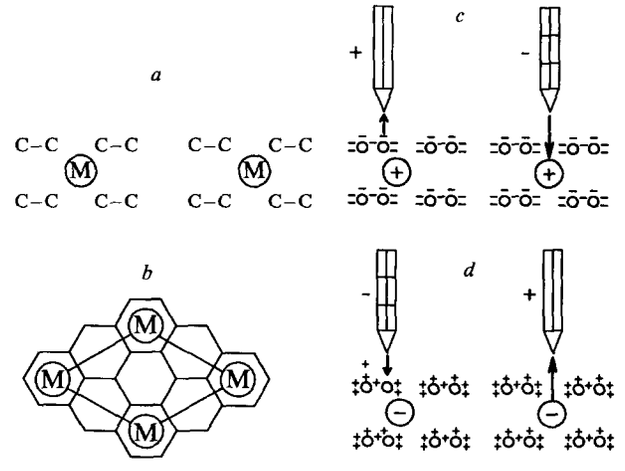


Figure 2. (2×2) structure of an intercalation graphite compound of the MC_8 type.[34, 35]
(*a*) transverse section; (*b*) top view of the basal plane; localisation sites of the tunnelling electrons in compounds of graphite with electron donors (*c*) and acceptors (*d*) for different polarities of the tunnelling voltage.

inhomogeneous regions determined by the method of preparing the graphite. The structure of the carbon fibre also depends on the method of synthesis, and on the temperature of heat treatment. For example, high-temperature graphitisation of the fibre results in ordering of the structure at the atomic level, as is clearly shown by the STM pictures.[47]

Scanning tunnelling microscopy has been used successfully in studies of the processes involved in the etching of the basal plane of graphite during the gasification of HOPG in air.[50, 51] This work has made clear the unique possibilities of the method in studies of reaction kinetics at the molecular level.

Heating a clean, freshly cleaved HOPG surface at 773 – 873 K in air produces a uniform distribution of circular etch pits one monolayer deep over the surface. The concentration of these pits varies between 0.1 and 13 μm^{-2} in different samples. Their diameter (but not their number) increases linearly with the time of heat treatment. The rate constant for the removal of carbon on one active centre calculated[50] from kinetic data is 0.5 s^{-1}. A typical activational temperature dependence of the growth rate of the diameter for the monolayer etch pits has been observed[51] between 773 and 973 K. The activation energy determined from these data is 127 kJ mol^{-1}, which is close to the value[51] obtained gravimetrically (147 kJ mol^{-1}). Successive heating and cooling cycles increase the size of the old pits as well as producing new pits. Therefore the etching is controlled by the presence of vacancies or impurities on the surface. Increasing the heat treatment temperature above 973 K produces a large number of concentric pits one monolayer deep, and at 1173 K the STM picture consists of conical craters.

Many different types of tracks, channels, and craters are seen on samples which have been stored in air for long periods or exposed to chemically active (or even inert) materials before being heat treated. Since in these cases the STM pictures are independent of the nature of the impurity on the HOPG surface it has been suggested[50] that the carbon gasification centres may be formed by the mechanical interaction of the impurity particles and the graphite particles.

2. Metals

Attempts to achieve a resolution sufficient to observe atoms on a clean metal surface have long been unsuccessful, though some workers have observed monatomic steps and reconstructions of the surface of single crystals induced by gases.[52–54] The lack of resolution on an atomic scale on metallic surfaces has been interpreted as a manifestation of the high level of delocalisation of the electron density in metals. The first report of atomic resolution on a close-packed surface of monocrystalline gold was published[55] in 1987. The anomalously high amplitude (up to 0.5 Å) of the atomic corrugations was stressed. By analogy with graphite this phenomenon was ascribed to the presence of local surface states near the Fermi level. In the following year another group of workers[56] proposed a different explanation of the atomic resolution which they had observed on an Al(111) monocrystal. A reasonably reproducible method of modifying the point of the STM to give an enhanced resolution was proposed: it was based on the experimental observation that the point is elongated by ~25 Å when a pulse of increased tunnelling voltage is applied to it over a gold or aluminium sample. It was suggested that this pulse induces the transfer of a small cluster of material from the substrate to the tip of the needle, thus increasing the contrast of the image. The same workers attribute the anomalously high corrugations to elastic deformations of the resulting cluster by the interatomic forces which it experiences from both sides (the needle and the sample).

Different theoretical interpretations of the anomalous amplitude of the atomic corrugations on metal surfaces have already been proposed. According to one of these the resolution of a tungsten needle[57] can be ascribed to the elimination of all impurities from the needle, giving ideally clean tungsten, whose d_{z^2} atomic function has a smaller radius of curvature than the generally adopted s wave function model of the electronic structure of the point. An alternative theory[58] postulates that for small tunnelling gaps (in which the atomic corrugations of metals surfaces are observed) large changes in the electronic structure of the surface can take place, and the tunnelling current can no longer be assumed to flow between unperturbed electronic states In this case localised electronic states induced by the point above the Fermi level appear on the surface. It was shown that their energy distribution and the effective height and width of the tunnelling barrier are very different in the regions above the atoms and above the vacancies. As a result the contrast of the STM representation of the metal surface increases until atomic resolution is achieved. The amplitude of the atomic corrugation calculated by this model (~0.3 Å) is close to the experimentally observed value (0.1 – 0.5 Å).

The achievement of resolution on an atomic scale on metals stimulated new studies of metal surfaces, including processes leading to their reconstruction. The positions of the atoms on a reconstructed metal were first established for the (111) gold surface.[59, 60] We know that gold is the only metal with a face-centred cubic (f.c.c.) packing in which reconstruction of the (111) face into a hexagonal close-packed (h.c.p.) structure is observed. Woll et al.[59] and Barth et al.[60] were able to visualise $(23 \times \sqrt{3})$ elementary cells forming a structure of parallel lines (Figure 3*a*). A more detailed study[60] also revealed superstructures identified as 120° breaks in the lines approximately 250 Å apart, producing a zigzag pattern in the STM (Figure 3*b*). Surface steps and bulk defects do not impede the passage of the lines, though they affect the details of the picture. It is interesting to note that these lines are always closed. These results suggest a model of the reconstruction consisting in a transition from f.c.c. to h.c.p. packing in the upper atomic layer.

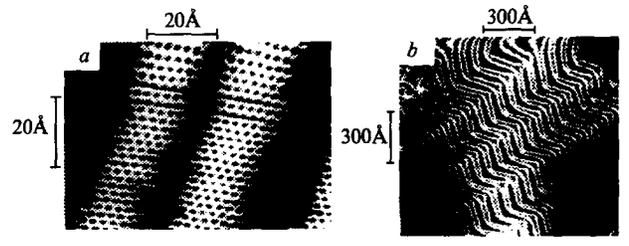


Figure 3. STM image[60] with atomic resolution of the reconstructed Au(111) surface.
(*a*) structure of parallel lines, the frame defines the elementary $23 \times \sqrt{3}$ cell, difference in height between the black and the white areas 0.2 Å; (*b*) structure of the zig-zag lines.

Scanning tunnelling microscopy results have also shown[61] that carefully prepared, clean (110) faces of platinum and gold undergo a thermodynamically stable (1×2) reconstruction by the 'absent rows' model rather than through impurity effects (Figure 4). The (1×2) reconstruction remains stable even near a screw dislocation. Increasing the concentration of impurity (mainly calcium) decreases the relative proportion of regions with a (1×2) structure and increases the proportion of (1×7) and (1×5) structures. Ultimately, at high impurity concentrations, we obtain a (1×3) structure consisting of (111) micro-facets.

An analysis of sequential STM representations of an Au(110)-(1×2) structure, obtained in a period of several hours in an ultra-high vacuum,[62] revealed a substantial motion of the surface atoms. The structural changes were found to be related to defects on the steps (i.e. to kinks) on the (100) microfacets, confirming the earlier hypothesis of an important contribution to mass transfer from these defects.

A study of the fine structure of the steps on an Ag(111) face showed that at room temperature this structure includes an irregularity of subatomic dimensions, indicating a motion of the atoms along the steps between successive frames of the scan.

Lowering the temperature to 27 K in order to lower the mobility of the atoms removes the kinks from the steps.

In situ studies by STM of the Ag(111) surface gave visual evidence[64] that an increase in temperature converts an initially regular (though stepped) surface into a disordered system as a result of the surface diffusion of atoms, with an effective transition temperature of ~350 K. The list of metals which have been studied by STM is continually growing. In particular, studies of chromium monocrystals have been reported.[65, 66]

Studies of the interaction of gases with the structure of the surface are of special interest. These are conveniently classified into two groups. The first includes the visualisation of adsorbed molecules and the identification of their adsorption sites, the second deals with surface reconstruction processes induced by gases.

The adsorption sites of the molecules can be determined only when the STM offers atomic resolution. One of the earliest studies of the adsorption of oxygen[67] was carried out on an Al(111) monocrystal surface. Even at low coverages (up to 5% of a monolayer) islets of adsorbed oxygen uniformly distributed over the surface can be distinguished, but they appear as depressions 10–20 Å in diameter rather than as prominences. This confirms that the STM image describes the local distribution of electron density. After being annealed at 800 K the sample shows some characteristic surface formations: a mound surrounded by a ring of six depressions, with three aluminium atoms round each depression. These structural features were interpreted as oxide nuclei.

The STM image of molecules adsorbed on a substrate is the result of changes in the local electron density not only at the site of the adsorbate but also on the neighbouring atoms of the substrate, as was demonstrated[68] for carbon atoms adsorbed on Al(111). As can be seen from Figure 5, the carbon atom adsorbed on a hexagonal metal lattice has a trigonal symmetry. The images of the six aluminium atoms nearest to this carbon atom differ markedly from those of the more remote atoms. Three of them are bound to the carbon and appear as pits, whereas the other three seem to project above the surface. The authors conclude from these results that the apparent changes in the vertical position of the aluminium atoms are more probably due to a redistribution of the electron density than to genuine structural changes.

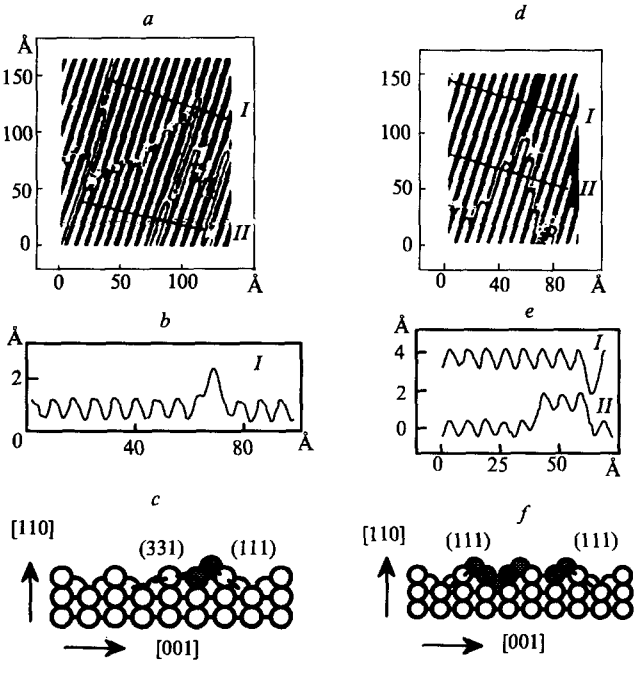


Figure 4. STM images[61] of the reconstructed Au(110) surface.
(*a*) top view of the region with a (1 × 2) structure; (*b*) transverse section along the line *I* shown in Figure 4*a*; (*c*) model of the structure of the surface along the line *I*, showing the structure of the microfacets; (*d*) top view of the region of the surface with (1 × 2) and (1 × 3) structures; (*e*) transverse sections along the lines *I* and *II* shown in Figure 4*d*; (*f*) model of the structure of the surface along the lines *I* (open circles) and *II* (filled circles).

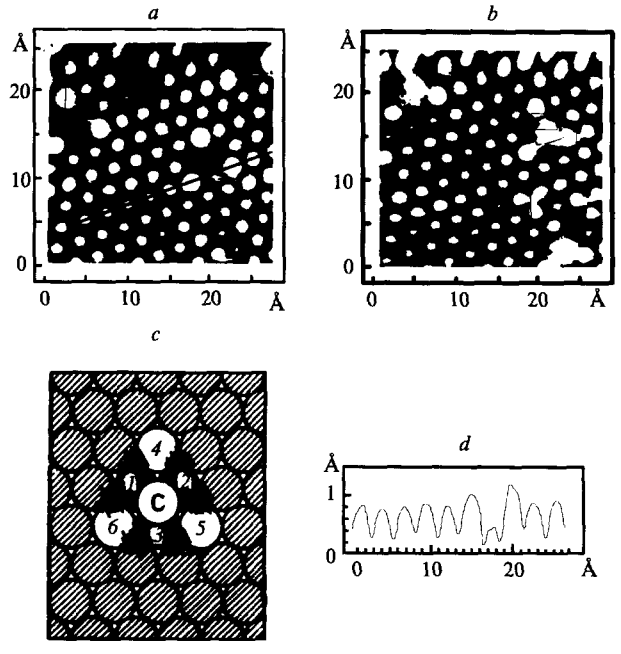


Figure 5. Successive STM representations[68] of the Al(111) surface with adsorbed carbon atoms.
(*a*) $V = -20$ mV, $I = 41$ nA; (*b*) $V = -70$ mV, $I = 41$ nA; (*c*) model of the atomic surroundings of an adsorbed carbon atom; aluminium atoms of the first (*1*–*3*) and of the second coordination sphere are shown (*4*–*6*); (*d*) transverse section along the [110] direction shown in Figure 5*a*.

The scanning tunnelling microscopy method has also been used[69] in studies of the adsorption of oxygen on a Ni(100) single crystal. At 400 K and 15% coverage square pits with a side of ~4 Å were found in the STM pictures, and ascribed to oxygen atoms. These pits are located over cavities of the square nickel lattice. Unlike the oxygen atoms adsorbed on Al(111) the oxygen atom on Ni(100) do not tend to form islets and appear to be uniformly distributed over the surface. However, a more detailed study revealed some ordering of the adatoms on the surface. Statistical evidence of interaction between the adatoms up to the third nearest neighbour was obtained. Gradually increasing the coverage of the surface produces first a $p(2 \times 2)$ and then a $c(2 \times 2)$ packing of the adsorbed layer.

Studying the distribution of the adsorbed molecules over the surface gives information on their interaction. Thus, the formation of sulfur clusters on the Re(0001) face has been observed[70, 71] in this way. At low surface coverages (up to 25% of a monolayer) the sulfur atoms are located over the c.p.h. cavities of the Re lattice, forming $p(2 \times 2)$ or (less often) $c(\sqrt{3} \times 5)$ structures. At higher surface loadings the more close-packed $(\sqrt{3} \times \sqrt{3})R30°$ structure is replaced by clusters of three, four, or six atoms, but not by dimers, indicating the presence of three-centre interaction. The authors suggest[70, 71] that this interaction takes place through the substrate, because the distance between the sulfur atoms in the clusters is much greater than the interatomic distance in the S_2 and S_8 molecules. This assumption is also confirmed by the absence of a similar effect when the S/Mo(001) system is studied in the air.[72]

Scanning tunnelling microscopy has been successfully applied in a study of the structure of surfaces during the adsorption of

aromatic compounds. Ordered (3×3) circular formations, occasionally with a resolved fine structure ascribed to benzene rings, have been observed[73] in the coadsorption of benzene and CO (up to saturation) on a Rh(111) surface. In a study of the adsorption of naphthalene on Pt(111) it was found[74] that the adsorbed molecules can be accommodated in three positions differing by a 120° rotation of the molecule in the plane. At low coverages the naphthalene molecules are distributed uniformly, and they can rotate round their axis and move over the surface, as was demonstrated by comparing successively recorded STM pictures. The mobility of the adsorbate is greatly suppressed at higher coverages.

With large molecules the site of attachment to the substrate is difficult to determine, because several such sites may be involved, but under these conditions the visualisation of the molecule by STM can be improved until the structure of the molecule is resolved. Thus, the electron density distribution in copper phthalocyanine adsorbed on a Cu(100) substrate has been established in this way.[75] It was pointed out that this was made possible only by a correct choice of the metal support, since the phthalocyanine molecule can move along the surface (like silver phthalocyanine on a polycrystalline silver foil[76]).

The adsorption of molecules is often accompanied by reconstruction of the surface, but different types of reconstruction can be encountered, depending on the nature of the adsorbate and of the metal, on the type of face, on the temperature and on the coverage.[77]

The O/Cu system has been studied most intensively by scanning tunnelling microscopy.[78–83] On the STM pictures of the clean Cu(110) surface the monatomic steps were found to have the shape of a fringe.[78] This was interpreted as evidence of a substantial amount of diffusion of the copper atoms over the surface. Quantitative estimates of the diffusion coefficient obtained from successive STM pictures showed that a monolayer of copper adatoms (removed from the steps) can be formed in less than 20 s at room temperature. When adsorbed oxygen is present on the surface the wandering copper adatoms are captured by the oxygen atoms and the surface is reconstructed, giving a (2×1) structure formed from O–Cu–O chains extending above the base plane and oriented in the [001] direction. At higher coverages the chains combine into islets elongated in the same direction, denoting a greater probability of capture of the wandering adatom at the end of the chain than on its side. The larger islets are less mobile, but individual chains can be captured by them to produce even larger islets. By visualising the dynamics of this process[79] at about 1 frame s^{-1} it can be shown that copper atoms are transferred from the steps to the terraces on the surface. This leads to the so-called additional rows model, which differs from the missing rows model by stipulating mass transfer in the opposite sense. At even greater exposures the (2×1) structure is converted into a $c(6\times2)$ structure. In this case the formation of islets of the new structure beings on the steps.

Unlike the Cu(110) face, the Cu(100) gives a $(2\sqrt{2}\times\sqrt{2})R45°$ structure under the influence of oxygen. Under these conditions successive STM pictures show[80] that the nucleation and growth of islets takes place on the terraces, and that the steps are almost unaffected. The islets grow preferentially in the [010] and [001] directions. This is taken[80] as direct evidence that the reconstruction of the (100) face takes place by the missing rows model with formation of O–Cu–O chains in the [001] direction, which then coalesce in the [010] direction to give islets.

Two previously unknown structures containing 29 and 44 (1×1) cells respectively have been discovered[84] in the O/Cu(111) system. They were ascribed to the mixing of the hexagonal lattice of the $Cu_2O(111)$ face with the (1×1) copper lattice.

Surface reconstruction under the influence of alkali metals is well known, but only one study of this effect has so far been reported:[85] the mechanism of the reconstruction of the Cu(110) face induced by potassium. It was shown that at low coverages the potassium atoms are uniformly distributed as single atoms or as chains of 2 or 3 atoms in the [110] direction, and that these species (unlike oxygen) are not captured by surface steps. It is suggested that copper atoms under the potassium atom are squeezed out and migrate along the surface, ultimately landing on steps. Increasing the coverage to 15% of a monolayer results in growth of the chains, with formation of (1×4) and (1×3) structures. At still higher coverages the reconstruction ceases and the well known (1×2) structure is observed.

STM studies of the morphology of Pt(111) samples after the ion bombardment and annealing[86, 87] have made an important contribution to our understanding of the role of defects in surface processes. Irrespectively of the nature of the ion (He^+, or Ar^+) trigonal craters are formed on the metal surface at low doses and for annealing temperatures below 700 K. Increasing the annealing temperature results in the formation of monolayer pits and islets, whether the anneal is carried out during the bombardment or after it. This shows that an increase in temperature produces a substantial mass transfer between the layers. The islets formed under these conditions have a trigonal symmetry, indicating thermodynamic equilibrium. It is assumed[86, 87] that these processes are common to all metals with an f.c.c. lattice [at least, on the (111) face].

Real polycrystalline systems have not been studied in depth so far. They were used as samples during the initial stages of the development of tunnelling microscopy. Thus, Gimzewski et al.[88] compared the topographies of silver films evaporated on substrates at different temperatures with the aim of establishing the effect of surface roughness on the enhancement in hyper Raman scattering. Some studies of the epitaxy of metallic layers on metals should also be noted.[89]

The above STM studies of metals were carried out on monocrystalline samples under vacuum conditions, in conjunction with data obtained by electron-spectroscopy and structural methods of analysis such as low-energy electron diffraction, Auger spectroscopy, X-ray spectroscopy, UV electron spectroscopy, etc. Of course, under these conditions the information content of the scanning tunnelling microscopy method is substantially enhanced. Comparing different methods allows us to use scanning tunnelling microscopy in cases where alternative methods are unsatisfactory, for example owing to the small size of the metallic particles, to their very low concentration, or to their amorphous structure.

3. Clusters and small particles

The development of tunnel microscopy has stimulated considerable interest from workers engaged in the study of clusters. Applying STM to cluster studies usually involves the following steps: depositing the substance of interest on a flat, electrically conducting substrate in concentrations low enough to allow the atomic structure of the substrate to be observed; a quantitative element analysis of the composition of the surface; visualising the particles in the STM. In spite of the apparent simplicity of this approach only a few studies of clusters by scanning tunnelling microscopy have been reported. Difficulties are met even at the stage of choosing a substrate. A clean surface and ultra-high vacuum conditions are needed when monocrystals of metals or of semiconductors (of the silicon type) are chosen. In this respect pyrolytic graphite is more convenient, but (as was said above) there may be problems in interpreting the STM representation because of the possible formation of anomalous superstructures on the graphite substrate. Difficulties are also met in ensuring uniform deposition of the clusters because of the possibility of very rapid diffusion on the inert pyrographite surface, and also of uneven evaporation of the solvent when the clusters are deposited from a solution. Lastly, treating HOPG with acetone produces a regular structure with a period of ~4 Å (which eventually disappears), and treatment with a solution of $[Et_4N]_3[Re_7C(CO)_{21}]$ in acetone produces a hexagonal structure with a period of 10 Å in addition to amorphous aggregated formations.[90]

A more uniform distribution of the particles is obtained by molecular beam deposition in a stream of inert gas or by thermal evaporation in a vacuum, with condensation of the atoms on a substrate. Ligand-free particles of different size can be obtained by varying the deposition conditions. Clusters with a ligand coat and molecular complexes are usually deposited from solutions on a graphite or gold substrate. Often the deposition of the particles and the element analysis of the surface are carried out in a vacuum, and the STM study in the air (sometimes including a repeated check for changes in composition of the surface during the vacuum treatment). However, some ambiguity in the interpretation of the results cannot be avoided in these experiments.

The potential advantages of STM in studies of small particles were first demonstrated by the observation of isolated particles of silver, gold, and aluminium on a graphite substrate.[91, 92] In spite of the high mobility of the adatoms relatively stable single atoms of the metal could be detected near the larger particles. Dimers and linear trimers were also seen in the STM pictures. It should be noted that atoms were never observed over the cavities in the graphite lattice: from this result, and from an analysis of the interatomic distances, the authors suggested the presence of a strong interaction between the metal and the carbon substrate, which is suppressed by increasing the size of the particle.

This conclusion was tested by statistical studies[93] of the position of the metal atoms, and by determining the length of the metal–metal bonds in the platinum dimers and trimers. It was found that the position of the metal atoms was stable in time. An analysis of the position of the single metal atoms with respect to the graphite lattice showed that no preferential binding site could be identified, though the metal atom had the highest probability of lying above a carbon atom not directly bound to the lower layer. The average Pt–Pt distance in the dimers was 2.45 ± 0.26 Å, i.e. close to the lattice parameter of the graphite. However, the relatively wide distribution of the Pt–Pt bond lengths made it impossible to establish unambiguously whether this agreement was fortuitous or whether it was the result of platinum–carbon interactions. The trimers were mostly linear, or arranged as equilateral triangles. The average bond length of the trimers was 2.66 ± 0.32 Å, suggesting a predominant effect from the metal–metal bonds.

Humbert et al.[94] studied clusters of gold and palladium deposited by the atomic beam method in a Knudsen cell on a single crystal of natural graphite at 623 K. Under these deposition conditions the particles grow as a result of the diffusion of adatoms over the surface. According to transmission electron microscopy results the particles were condensed mainly along the graphite steps. The STM images revealed both large (~100 Å) and small particles (~15 Å), with a ratio of height to diameter of ~0.1, indicating a strong compression of the particles.

The preferential formation of flat structures is confirmed by a statistical analysis of more than 200 particles of platinum on graphite at different coverages. When the coverage is increased from 10% to 50% of a monolayer the particle diameter increases from 47 to 80 Å, whereas the average height (3.8 Å) stays practically constant. Unfortunately, these results were obtained by working in the air, which gave an oxygen content of the surface 3–4 times higher than in the initial sample immediately after evaporation of the metal. Therefore it is not clear whether the results apply to particles of platinum or of its oxide.[95]

In order to establish the effect of exposure to air on the observed form of the clusters Humbert et al.[96] compared the STM pictures obtained by depositing palladium particles in a vacuum and in air. The clusters were deposited by the atomic beam method on to a graphite substrate heated to 573 K, previously irradiated in a low-energy (50 eV) ion beam with a dose of less than 10^{12} ions cm^{-2} in order to increase the concentration of adsorbed particles on the surface. According to those workers the shape of the larger particles (> 100 Å) was unaffected by deposition in air. On the other hand an unexplained corrugation of atomic dimensions was seen on the surface of the smaller particles (15 Å) in air.

Clusters of gold deposited by a molecular beam on an atomically flat gold substrate were used to examine possible explanations of the compression of the particles observed in the STM, including artefacts associated with the production of the STM image.[97] The authors concluded that the compression occurs only in particles of size smaller than a critical size determined by the nature of the substance. The compression is due to plastic deformation, which lowers the surface energy at the contact with the substrate.

More recent papers have described STM studies of large Au_{55} clusters stabilised by ligands[98, 99] and of Pd_{561} clusters,[99] deposited from solutions on HOPG or gold substrates. The difficulty of working with these materials is stressed: the surface mobility is high, especially on graphite, and the cluster can be entrained by the point until it is transferred to the needle of the microscope. Therefore the results so far are only tentative. Similar investigations of the visualisation of heteropoly acids (hydrogen tungstophosphate)[90, 100] and BiI_3 clusters[101] have been reported.

A new class of carbon compounds (the fullerenes) has recently come to the fore in the study of clusters. Their properties have been studied by various physical methods, including scanning tunnelling microscopy.[102, 103] After mild evaporation of C_{60} and C_{70} clusters on to a gold substrate regular close-packed spherical structures spaced at a distance of ~11 Å between centres were observed on the surface. Furthermore after deposition on the Au(110) face [but not on the (111) face] C_{60} showed intramolecular structure both in air and in an electrochemical cell containing a solution of $HClO_4$.[104] A model of the electron tunnelling which allows for superexchange interactions was developed from the STM images obtained in this work.

The present writers believe that studies of clusters and of small particles by scanning tunnelling microscopy will develop mainly in the following directions: the achievement of intramolecular resolution (for example, at low temperatures); studies of the dynamics of the cluster behaviour in adsorption processes and during changes in temperature; studies of electronic structure. All these directions need new theoretical models to be developed in order to interpret the STM representations of the clusters.

4. Model catalysts

Alumina or silica are often used in industrial catalysts as carriers with a highly developed surface. Unfortunately these carriers are electrically insulating, and therefore the catalysts cannot be studied by scanning tunnelling microscopy. Substrates of carbon materials or of 3*d* metal oxides have been used for STM studies of model catalysts. Studies of transition-metal oxides are also of independent interest because these materials are themselves catalysts for many processes. Titanium oxide has been studied most intensively by scanning tunnelling microscopy.

The TiO_2 surface partially reduced in hydrogen has been studied in air as a function of the conditions of surface treatment (polishing and etching),[105] and the effect of the potential applied to the sample in an electrochemical cell on the STM picture has also been examined.[106] It was found that stable images of *n*-TiO_2 are obtained only when negative potentials are applied to the sample, suggesting a system of energy bands typical of semiconductors. The band structure of the oxide was established by tunnelling microscopy (TS) on *n*-TiO_2(001) samples[107, 108] and reduced TiO_2(110) samples.[109] The measurements were made in air. The edges of the energy gap were determined from the tunnelling spectra.[107] A hysteresis observed[108] in the tunnelling spectra was ascribed to surface states induced within the energy gap by the electric field.

From the tunnelling spectroscopy results the width of the energy gap was found[109] to be only 1.7 eV [(+0.25)–(–1.35) eV relative to the Fermi level], i.e. much smaller than the bulk value (~3.0 eV). (The possibility of this effect being due to the presence

of a large number of states near the band edges cannot be excluded, since the measurements were made in air.) Of course, a stable STM picture cannot be obtained when the applied tunnelling voltage brings the Fermi level of the metal of the needle within the forbidden band of the oxide. However, the adsorption of phenol, for example, on the titanium oxide surface produces a surface state within the energy gap ~0.45 eV below the Fermi level. Scanning for this potential difference produced STM images of the phenol, which appeared to be adsorbed parallel to the plane of the oxide. These workers adopted the approach used in scanning tunnelling spectroscopy: they scanned the sample at a predetermined tunnelling voltage.

Rohrer et al.[110] obtained atomic resolution on a sample of reduced $TiO_2(110)$ by careful surface preparation and by operating the STM in an ultra-high vacuum. The STM image showed some clearly developed lines alternating (with a period of 8.5 Å in the [111] direction) with a less well developed corrugation having a period of 3.4 Å along the lines. This picture was interpreted as an ordered packing of two-dimensional defects (crystal lattice shifts).

As in the case of titanium oxide, atomic resolution could not be obtained in an STM study[111] of ZnO(0001) monocrystals. Attention was paid mainly to the effect of surface geometry on the electronic structure of the surface. The STM pictures of the ZnO crystal contained a large number of steps in the [1010] and [1120] directions. The tunnelling spectroscopy results suggest that these steps lead to the formation of surface states in the forbidden energy gap which are probably responsible for the chemical reactivity of the surface.

The scanning tunnelling microscopy method can be used to study strong metal–substrate interactions. According to one of the models the effect is caused by the decoration of the metallic particle by the carrier, with formation of new active centres on the metal–oxide interface. One approach to the study of these interactions is to use oxide samples deposited on a metallic substrate (i.e. a reversed-phase model of the catalyst), because the electrical conductivity of the oxides is low and the effects of surface charge are substantial.

Thus, STM has been used[112] to study islets of MnO_x deposited on a Ni(111) substrate during the adsorption of CO. Measurements of the perimeter of the particles as a function of the mean coverage revealed a correlation with data for the thermal desorption of CO. These results confirm the earlier conclusion that the increased rate of hydrogenation of CO is associated with the CO adsorption centres at the metal–oxide interface.

Islets 20 Å in diameter, in the form of rings, were observed[113] on Rh(111) at submonolayer coverages of TiO_x. The ring shape was obtained only when negative tunnelling voltages were applied to the sample, and therefore its origin must be electronic. These observations were explained in terms of partial reduction of the TiO_2 at the perimeter of the particle.

Unlike TiO_2 zirconium oxide (ZrO_2) is not easily reducible as a substrate. ZrO_2/Pd(100) systems have been studied by scanning tunnelling microscopy. The results[114] suggest the presence of different types of region in this system. The first is assigned to metallic palladium, the second to semiconducting zirconium oxide. The third region is seen only on samples prepared by thermal oxidation in air at 673 K of $Zr(OC_2H_5)_4$ sublimed on a Pd(100) substrate. According to EXAFS spectroscopy results this region may be associated with palladium oxide. It has been suggested that in an oxidising atmosphere the zirconium oxide is uniformly distributed over the whole surface of the substrate. After treatment in hydrogen at 773 K for one hour the oxide islets develop a bulk structure with a sharp metal–oxide boundary. It is suggested that this boundary prevents the decoration of the metal particles by the reduced oxide when zirconium oxide is used as the carrier.

One method of visually resolving the phases in the STM picture relies on the large difference in work function between the metal and the substrate. This conclusion was reached in one of the first studies of model catalysts: ultra-dispersed particles of gold and platinum on carbon substrates, and of titanium oxide.[115] The same approach was used in the Pt/Ga_2O_3 system.[116] The metal particles were identified with a greater contrast by superposing the $\varphi(x, y)$ distribution map on the topogram of the same area of the surface. By comparing the maps thus obtained before and after an anneal of the sample at 1100 K large differences in the structure of the sample were detected. Before the anneal the platinum islets were circular and of similar size, but after being annealed the surface developed a patchwork appearance with the islets concentrated mainly along the grain boundaries of the Ga_2O_3: this may account for the decrease in the free platinum surface (according to Auger spectroscopy results) and in the catalytic activity towards the oxidation of CO (according to mass spectrometry results).

It is well known that catalytic activity is largely determined by the method of preparation of the catalyst: its previous history, and its treatment and conditioning. Therefore studies of all these stages are of interest. In this respect the studies of the effect of various pretreatments on the morphology of platinum particles on a graphite surface are particularly meaningful.[117,118] The particles were obtained by various methods, including the reduction in hydrogen of tetrachloroplatinic(II) acid H_2PtCl_4 or of tetra-ammineplatinum nitrate for 2 h at 723 K. A graphite surface (clean, or treated with nitric acid for 50 h at room temperature) was used as substrate. Detailed studies by STM were carried out at each stage. Thus, the modification of graphite by HNO_3 produced a more uniform distribution of the precursor, and the platinum salt gave smaller associations than the H_2PtCl_4. The size and the distribution of the reduced particles were less dependent on the nature of the precursor, but their microstructure and morphology were strongly influenced by the previous history of the sample. Thus, in the reduction from tetra-ammineplatinum on a substrate treated with HNO_3 the reconstruction of the platinum surface into a structure close to $(111)(\sqrt{3} \times \sqrt{3})$ induced by atmospheric oxygen was visualised for the first time for small particles.

The dynamics of the changes in the morphology of the particles on a graphite surface during the reduction of platinum from H_2PtCl_4 were studied under conditions analogous to those used in the preparation of the platinum catalyst.[118] It was shown that for short reduction times (0.5 h, 723 K) rod-shaped particles are formed, both large (1000–2000 Å long and 100–500 Å high) and small (280 Å long and 30 Å high). This large scatter suggests a partial reduction of the precursor. After being reduced for 2 h the particles break down into crystallites, ellipsoid in shape, and ultimately (after 60 h) they produce particles with a nominal diameter of ~170 Å and ~20 Å high, showing a well faceted surface. On the other hand the platinum particles evaporated in a vacuum and treated with hydrogen at 623 K for 0.5 h are spherical, with a diameter of 25–100 Å and an atomically disordered surface structure.

The study of the shape of the particles reduced from H_2PtCl_4 for different times showed that the crystallite shape is determined mainly by the reduction conditions and is less dependent on the precursor, on the type of graphite substrate, and on the method of deposition. It was found that a small proportion of the crystallites is spherical (with a ratio of length to width not greater than 1.2), and that the proportion of these increases with the reduction time though not above 40%. This is surprising, since crystallites of platinum in thermodynamic equilibrium (a metal with an f.c.c. structure) should be spherical. Studies of the degree of sphericity of the particles could be of interest in relation to the thermodynamics of small supported particles.

Molybdenum disulfide occupies a special place among model catalysts, because it has a layer structure similar to that of graphite, built of S–Mo–S packets. The atomically flat surface of MoS_2 makes this a convenient substrate for visualising deposited molecules; furthermore molecules can, in principle, be intercalated between the layers, and this should help to explain

the nature of superconductivity in structures of reduced dimensionality (see Heckl et al.[119]). The strong localisation of the electron density makes atomic resolution possible, confirming the hexagonal packing of the upper layer.[120] However, the element which appears in the STM image has not yet been identified.[121–123]

Monolayer particles of MoS_2 deposited on a pyrolitic graphite substrate have been studied in this way.[123] It was found that if the layer of sulfide is surrounded by water molecules its surface undergoes a (2×1) reconstruction. When the sample is dried an STM picture identical to that of the surface of the bulk crystal is observed. By combining the results obtained from STM and EXAFS measurements the authors constructed a model in which the molybdenum had distorted octahedral surroundings in solvated samples. The aim of those studies was to determine the mechanism of the action of hydrodesulfurisation catalysts.

Only a few studies of industrial catalysts by scanning tunnelling microscopy have been reported so far.[124–127] The first dealt with the surface topography of an iron–zirconium alloy (the precursor of an ammonia synthesis catalyst).[124]

Besenbacher et al.[125] observed a very dispersed structure in a passivated ammonia synthesis catalyst containing iron. In addition to pores and cracks they found parallel ridged structures corresponding to the crystallographic orientation of magnetite grains. They suggested that these lines appear in the STM as a result of the FeO/Fe epitaxy accompanying the passivation of the catalyst, and that they correspond to the [110] direction of the iron lattice.

Studies of the platinum–rhodium gauze catalyst used in HCN synthesis showed that the surface roughness of this catalyst varies with the conditions of the reaction.[126] However, the increase in the surface area of the catalyst during the activation calculated from STM data (as compared with the initial surface) was not more than two-fold, which is an order of magnitude less than the values obtained by other methods. Therefore the authors concluded that the main contribution to the increase in area is provided by the formation of crystallites more than 1 μm in diameter, and not by changes in morphology on a submicrometre scale.

Ex situ studies of the morphological changes in a supported Ag/SiC catalyst (for the conversion of ethylene glycol into glyoxal) were made possible by the formation of a conducting layer of silver over the whole surface of the carrier.[127] According to the scanning tunnelling microscopy results the silver particles are sintered into larger flat formations under the conditions of the reaction. Additions of small quantities of diethyl phosphite to improve the selectivity of the reaction produce a marked change in the topography of the catalyst, giving a surface of the fractal type, probably as a result of chemical erosion.

Thus tunnelling microscopy is often the only suitable method of studying catalytic systems. The amount of information which it yields on model catalysts depends on the specific properties of the system of interest.

* * *

The results discussed above show that scanning tunnelling microscopy is a powerful instrumental method of studying the surface of electrically conducting systems. Further improvements in the method for *in situ* temperature and adsorption studies and the application of the scanning tunnelling spectroscopy method in conjunction with fast scanning regimes should offer new prospects of studying the kinetics of surface processes at the atomic-molecular level.

References

1. G Binnig, H Rohrer *Rev. Mod. Phys.* **59** 615 (1987)
2. J G Simmons *J. Appl. Phys.* **34** 1793 (1987)
3. R Pool *Science* **247** 634 (1990)
4. R J Behm (Ed.) *Scanning Tunneling Microscopy and Related Methods* (Dordrecht: Kluver, 1989)
5. N S Maslova, V I Panov *Usp. Fiz. Nauk* **157** 185 (1989)
6. Y Kuk, P J Silverman *Rev. Sci. Instrum.* **60** 165 (1989)
7. V S Edel'man *Prib. Tekh. Eksp.* 5 25 (1989)
8. D W Pohl *IBM J. Res. Devel.* **30** 417 (1986)
9. J Bardeen *Phys. Rev. Lett.* **6** 57 (1961)
10. J Tersoff, D R Hamann *Phys. Rev. B* **31** 805 (1985)
11. J Tersoff *Phys. Rev. Lett.* **57** 440(1986)
12. N D Lang *Phys. Rev. Lett.* **55** 230 (1985)
13. N D Lang *Phys. Rev. Lett.* **56** 1164 (1986)
14. A Selloni, P Carnevali, E Tossati, C D Chen *Phys. Rev. B* **31** 2602 (1985)
15. C J Chen *J. Vac. Sci. Technol. A* **6** 312 (1988)
16. R J Hamers, R M Tromp, J E Demuth *Phys. Rev. Lett.* **56** 1972 (1986)
17. R M Tromp, R J Hamers, J E Demuth *Phys. Rev. B* **34** 1388 (1986)
18. R M Feenstra, J A Stroscio, A P Fein *Surf. Sci.* **181** 295 (1987)
19. J M Gomez-Rodriguez, J Gomez-Herrero, A M Baro *Surf. Sci.* **220** 152 (1989)
20. N Garsia *IBM J. Res. Devel.* **30** 533 (1986)
21. N D Lang *Phys. Rev. B* 37 10 395 (1988)
22. J K Gimzewski, R.Moller. *Phys. Rev. B* **36** 1284 (1987)
23. G Binnig, H Fuchs, Ch Gerber, H Rohrer, E Stoll *Europhys. Lett.* **1** 31 (1986)
24. S Park, C R Quate *Appl. Phys. Lett.* **48** 112 (1986)
25. I P Batra, N Garsia, H Rohrer, H Salemink, E Stoll, S Ciraci *Surf. Sci.* **181** 126 (1987)
26. J M Soler, A M Baro, N Garsia, H Rohrer *Phys. Rev. Lett.* **57** 444 (1986)
27. T Tiedje, J Varon, H Deckman, J Stokes *J. Vac. Sci. Technol. A* **6** 372 (1987)
28. D Tomanek, S G Louie, H J Mamin, D W Abraham, R E Thomson, E Ganz, J Clarke *Phys. Rev. B* **35** 7790 (1987)
29. T R Albrecht, H A Mizes, J Nogami, S Park, C F Quate *Appl. Phys. Lett.* **52** 362 (1988)
30. J E Bucley, J L Wragg, H W White, A Bruckdorfer, D L Worcester *J. Vac. Sci. Technol. B* **9** 1079 (1990)
31. M Kuvabara, D R Clarke, D A Smith *Appl. Phys. Lett.* **56** 2396 (1990)
32. P I Oden, T Thundat, L A Nagahara, S M Lindsay, G B Adams, O F Sankey *Surf. Sci.* **254** L454 (1991)
33. M Sawamura, J F Womelsdorf, W C Ermler *J. Phys. Chem.* **95** 8823 (1991)
34. S Kelty, Ch Lieber *Phys. Rev. B* **40** 5856 (1989)
35. C H Olk, J Heremans, M S Dresselhaus, J S Speck, J T Nicholls *J. Vac. Sci. Technol. B* **9** 1055 (1991)
36. S Gautier, S Rousset, J Klein *J. Vac. Sci. Technol. A* **6** 360 (1988)
37. A Selloni, C D Chen, E Tosatti *Phys. Scr.* **38** 297 (1988)
38. X.-R.Qin, G.Kirczenow *Phys. Rev. B* **41** 4976 (1990)
39. S Kelty, Ch Lieber *J. Vac. Sci. Technol. B* **9** 1068 (1991)
40. M S Dresselhaus *Intercalation in Layered Materials* (New York: Plenum, 1986)
41. R Coratger, A Claverie, F Ajustron, J Beauvillain *Surf. Sci.* **227** 7 (1990)
42. L Porte, C H de Villeneuve, M Phaner *J. Vac. Sci. Technol. B* **9** 1064 (1991)
43. G M Shedd, P E Russel *J. Vac. Sci. Technol. A* **9** 1261 (1991)
44. G J Vandentop, P A P Nascente, M Kawasaki, D F Olgetree, G A Samorjai, M Salmeron *J. Vac. Sci. Technol. A* **9** 2273 (1991)
45. V Elings, F Wudl *J. Vac. Sci. Technol. A* **6** 412 (1991)
46. L M Siperko *J. Vac. Sci. Technol. B* **9** 1061 (1991)
47. S N Magonov, H-J Cantow, J-B Donnet *Polym. Bull.* **23** 555 (1990)
48. W P Hoffman, V B Elings, J A Gurley *Carbon* **26** 754
49. N M D Brown, H-X You *Surf. Sci.* **237** 273 (1990)
50. H Chang, A J Bard *J. Am. Chem. Soc.* **113** 5588 (1991)
51. X Chu, L D Shmidt *Carbon* **29** 1251 (1991)
52. Y Kuk, P J Silverman *Appl. Phys. Lett.* **48** 1597 (1986)

53. G Binnig, H Rohrer, Ch Gerber, E Weibel *Surf. Sci.* **131** L379 (1983)
54. W Hosler, R J Behm, E Ritter *IBM J. Res. Devel.* **30** 403 (1986)
55. V M Hallmark, S Chiang, J F Rabolt, J D Swalen, R J Wilson *Phys. Rev. Lett.* **59** 2879 (1987)
56. J Wintterlin, J Wiechers, H Brune, T Gritsch, H Hofer, R J Behm *Phys. Rev. Lett.* **62** 59 (1989)
57. C J Chen *Phys. Rev. Lett.* **65** 448 (1990)
58. E Tekman, S Ciraci *Phys. Rev. B.* **42** 1860 (1990)
59. ChWoll, S Chiang, R J Wilson, P H Lippel *Phys. Rev. B* **39** 7988 (1989)
60. J V Barth, H Brune, G Ertl, R J Behm *Phys. Rev. B* **42** 9307 (1990)
61. T Gritsch, D Coulman, R J Behm, G Ertl *Surf. Sci.* **257** 297 (1991)
62. J K Gimzewski, R Berndt, R R Schlittler *J. Vac. Sci. Technol. B* **9** 897 (1991)
63. J F Wolf, B Vicenzi, H Ibach *Surf. Sci.* **249** 233 (1991)
64. J W M Frenken, R J Hamers, J E Demuth *J. Vac. Sci. Technol. A* **8** 293 (1990)
65. R Wiesendanger, H J Gunhterodt *Surf. Sci.* **235** 1 (1990)
66. N M D Brown, H-X You *Surf. Sci.* **233** 317 (1990)
67. J Wintterlin, H Brune, H Hofer, R J Behm *Appl. Phys. A* **47** 99 (1988)
68. H Brune, J Wintterlin, G Ertl, R J Behm *Europhys. Lett.* **13** 123 (1990)
69. E Kopatzki, R J Behm *Surf. Sci.* **245** 255 (1991)
70. D F Olgetree, R Q Hwang, D M Zeglinski, A Lopez Vazquez de Parga, G A Samorjai, M Salmeron *J. Vac. Sci. Technol. B* **9** 886 (1991)
71. R Q Hwang, D M Zeglinski, A Lopez Vazquez-de-Parga *Phys. Rev. B* **44** 1914 (1991)
72. B Marchon, P Bernhardt, M E Bussel *Phys. Rev. Lett.* **60** 1166 (1988)
73. S Chiang, R J Wilson, C M Mate, H Ohtani *J. Microsc.* **152** 567 (1988)
74. V M Hallmark, S Chiang, Ch Woll *J. Vac. Sci. Technol. B* **9** 1111 (1991)
75. P H Lippel, R J Wilson, M D Miller *Phys. Rev. Lett.* **62** 171 (1989)
76. J K Gimzewski, E Stoll, R R Schlitter *Surf. Sci.* **181** 267 (1987)
77. G A Somorjai *Catal. Lett.* **12** 17 (1992)
78. J Wintterlin, R Shuster, D J Coulman, G Ertl *J. Vac. Sci. Technol. B* **9** 902 (1991)
79. F Besenbacher, F Jensen, E Lagsgaad, K Mortensen, I Stensgaard *J. Vac. Sci. Technol. B* **9** 874 (1991)
80. F Jensen, F Besenbacher, E Lagsgaad, I Stensgaard *Phys. Rev. B* **42** 9206 (1990)
81. F M Chua, Y Kuk, P J Silverman *Phys. Rev. Lett.* **63** 386 (1989)
82. Y Kuk, F M Chua, P J Silverman *Phys. Rev. B* **41** 12 393 (1990)
83. R Feidenhansl, F Grey, M Nielsen, F Besenbacher, F Jensen, E Langsgaad, I Stensgaard, K W Jacobsen, J K Norskov, R L Johnson *Phys. Rev. Lett.* **65** 2027 (1990)
84. F Jensen, F Besenbacher, E Lagsgaad, I Stensgaard *Surf. Sci.* **259** L774 (1991)
85. R Shuster, J V Barth, G Ertl. *Surf. Sci.* **247** L229 (1991)
86. T Michely, G Comsa *Surf. Sci.* **256** 217 (1991)
87. T Michely, G Comsa *J. Vac. Sci. Technol. B* **9** 862 (1991)
88. J K Gimzewski, A Humbert, J G Bednorz, B Reihl *Phys. Rev. Lett.* **55** 951 (1985)
89. D D Chambliss, R J Wilson *J. Vac. Sci. Technol. B* **9** 928 (1991)
90. J V Lyding, J S Hubachek, G Gammie, S Scala, R Brockenbrough, J R Shapley, M P Keyes *J. Vac. Sci. Technol. A* **6** 363 (1988)
91. D W Abraham, K Sattler, E Ganz, H J Mamin, R E Thompson, J Clarke *Appl. Phys. Lett.* **49** 853 (1986)
92. E Ganz, K Sattler, J Clarke *Surf. Sci.* **219** 33 (1989)
93. U Muller, K Sattler, J Xhie, N Venkatesvaran, G Raina *J. Vac. Sci. Technol. B* **9** 829 (1991)
94. A Humbert, M Dayez, S Sanday, C L Chapon, C R Henry *J. Vac. Sci. Technol. A* **8** 311 (1990)
95. S Eppell, G S Chottiner, D A Scherson, G Pruett *Langmuir* **6** 1316 (1990)
96. A Humbert, M Dayez, S Granjeaud, P Ricci, C L Chapon, C R Henry *J. Vac. Sci. Technol. B* **9** 804 (1991)
97. Y Z Li, R Reifenberger, E Choi, R P Andres *Surf. Sci.* **250** 1 (1991)
98. C Becker, Th Fries, K Wandelt, U Kreibig, G Schmid *J. Vac. Sci. Technol. B* **9** 810 (1991)
99. L E C Van de Leemput, J W Gerritsen, P H H Rongen, R T M Smokers, H A Wierenga, H van Kempen, G Schmid *J. Vac. Sci. Technol. B* **9** 814 (1991)
100. B Keita, L Nadjo *Surf. Sci.* **254** L443 (1991)
101. D Sarid, T Henson, L S Bell, C J Sandrof *J. Vac. Sci. Technol. A* **6** 424 (1988)
102. R J Wilson, G Mejer, D S Bethune, R D Johnson, D Chambliss, M S de Vries, H E Hunziker *Nature (London)* **348** 621 (1990)
103. J L Wragg, J E Chamberlain, H W White, W Kratchmer, D R Huffman *Nature (London)* **348** 623 (1990)
104. Y Zhang, X Gao, M J Weaver *J. Phys. Chem.* **96** 510 (1992)
105. S E Gilbert, J H Kennedy *J. Electrochem. Soc.* **135** 2385 (1988)
106. K Itaya, E Tomita *Chem. Lett.* **2** 285 (1989)
107. F-R Fan, A J Bard *J. Phys. Chem.* **94** 3761 (1990)
108. S E Gilbert, J H Kennedy *Surf. Sci.* **225** L1 (1990)
109. K Sakamaki, S Matsunaga, K Itoh, A Fujishima, Y Gohshi *Surf. Sci.* **219** L531 (1989)
110. G S Rohrer, V E Henrich, D A Bonnell *Science* **250** 1239 (1990)
111. G S Rohrer, D A Bonnell *Surf. Sci.* **247** L195 (1990)
112. Y B Zhao, Tz-S Lin, Y-W Chung *J. Catal.* **125** 207 (1990)
113. H Ch Wang, D F Olgetree, M Salmeron *J. Vac. Sci. Technol. B* **9** 853 (1991)
114. K Asakura, Y Iwasawa, S K Purnell, B A Watson, M A Barteau, B C Gates *Catal. Lett.* **15** 317 (1992)
115. M Komyama, S Morita, N Micoshiba *J. Microsc.* **152** 197 (1988)
116. W Hanreider, A Scholz, H Meixner *Surf. Sci.* **243** 166 (1991)
117. K L Yeung, E E Wolf *J. Vac. Sci. Technol. B* **9** 798 (1991)
118. K L Yeung, E E Wolf *Catal. Lett.* **12** 213 (1992)
119. W M Heckl, F Ohnesorge, G Binnig, M L Specht, M Hashmi *J. Vac. Sci. Technol. B* **9** 1072 (1991)
120. G W Stupian, M S Leung *Appl. Phys. Lett.* **51** 1560 (1987)
121. M Weimer, J Kramar, C Bai, J D Baldescwiller, W J Kaiser *J. Vac. Sci. Technol. A* **6** 336 (1988)
122. T R Coley, W A Goddard III, C Baldescwiller *J. Vac. Sci. Technol. B* **9** 470 (1991)
123. X R Qin, D Yang, R F Frindt, J C Irwin *Phys. Rev. B* **44** 3490 (1991)
124. R Schlogl, R Wiesendanger, A J Baiker *J. Catal.* **108** 452 (1987)
125. F Besenbacher, E Lagsgaard, I Stensgaard, P Stoltze, H Topsoe *Catal. Lett.* **8** 273 (1991)
126. B A Cowans, K A Jurman, W N Delgass, Y Z Li, R Reifenberger, T A Koch *J. Catal.* **125** 501 (1990).
127. P Gallezot, S Tretjak, Y Christidis, G Mattioda, A Schouteeten, Y-W Chung, T S Sriran *Catal. Lett.* 13 305 (1992)